




Self-healing alginate–carboxymethyl chitosan porous scaffold as an effective binder for silicon anodes in lithium-ion batteries

Zhao-Hui Wu, Juan-Yu Yang* , Bing Yu, Bi-Meng Shi, Chun-Rong Zhao, Zhang-Long Yu

Received: 16 April 2015/Revised: 28 May 2015/Accepted: 3 May 2016/Published online: 29 June 2016
© The Nonferrous Metals Society of China and Springer-Verlag Berlin Heidelberg 2016

Abstract Polymer binder plays a pivotal role in electrochemical performance of high-capacity silicon (Si) anode that usually suffers from severe capacity fading due to enormous substantial volume change of Si during cycling. In an effort to find efficient polymer binder that could mitigate such capacity fading, alginate–carboxymethyl chitosan (Alg–C-chitosan) composite polymer was investigated as a low-cost water-soluble binder for silicon anodes in lithium-ion batteries. The electrostatic interaction between carboxylate ($-\text{COO}^-$) of Alg and protonated amines ($-\text{NH}_3^+$) of C-chitosan forms a self-healing porous scaffold structure. Synergistic effect on the enhanced porous scaffold structure and self-healing electrostatic interaction of Alg–C-chitosan binder effectively can tolerate the tremendous volume change of Si and maintain an integrated electrode structure during cycling process. The Si nanopowder electrodes with Alg–C-chitosan composite binder exhibit an excellent cycling stability, with a capacity of $750 \text{ mAh}\cdot\text{g}^{-1}$ remaining after 100th cycling. In addition, an extraordinary areal capacity of $3.76 \text{ mAh}\cdot\text{cm}^{-2}$ is achieved for Si-based anodes with Alg–C-chitosan binder.

Keywords Binder; Alginate; Carboxymethyl chitosan; Self-healing; Scaffold; Silicon anode

1 Introduction

Silicon is a promising active material for anode in lithium-ion batteries, because it has the highest theoretical capacity

of $\sim 4200 \text{ mAh}\cdot\text{g}^{-1}$ for $\text{Li}_4\text{Si}_{22}$ [1, 2] and low charge–discharge potential of $<0.5 \text{ V}$ versus Li/Li^+ [3]. Nevertheless, the silicon anode materials suffer from severe volume change ($>400\%$) during the processes of Li^+ insertion and extraction [4, 5], and the unparalleled volume change of Si during battery operations leads to fatal fading mechanisms such as pulverization of active materials, loosened electrical contact between active materials and conductive carbon additives, slurry coating delamination from current collectors, as well as the excess growth of solid-electrolyte interphase (SEI) [6, 7]. As a result, the silicon anodes show fast capacity fading and low coulombic efficiency. While lots of nanostructured Si-based composite materials have been designed and synthesized [8–12], choosing a functional binder has also turned out to be an effective and low-cost method in mitigating these ruinous mechanisms.

As one of the major components of electrodes, polymeric binder is used to bind active materials and conduct additives together onto the current collector. The properties of polymeric binder play a vital role in maintaining the electrode structure during cycling, especially for silicon-based anodes. The most conventional binder poly(vinylidene fluoride) (PVDF) is widely used in commercialized lithium-ion batteries. The linear-type PVDF binder with inferior tensile strength attached to Si particles via weak van der Waals forces only cannot ensure good cycling performance to Si-based anodes [13, 14]. Recent researches show that synthetic and bio-derived polymers containing carboxylic acid and/or hydroxyl and/or amine functional groups and their derivatives, such as carboxymethyl cellulose (CMC) [15], carboxymethyl chitosan (C-chitosan) [16], poly(acrylic acid) (PAA) [17], alginate (Alg) [18], exhibit promising perspectives as binders for Si-based anodes. These functional binders show enhanced binding

Z.-H. Wu, J.-Y. Yang*, B. Yu, B.-M. Shi, C.-R. Zhao, Z.-L. Yu
Research and Development Center for Vehicle Battery and
Energy Storage, General Research Institute for Nonferrous
Metals, Beijing 100088, China
e-mail: juanyuyang@163.com

with silicon particles, and the chemical interactions between the polar functional groups of the binder and the partially hydrolyzed surface SiO_2 layer covering the silicon particles would prevent the anode from disintegration [19, 20], which explains the improved cycling stability of silicon-based anodes.

Moreover, it has been observed that polymeric binders with enhanced mechanical properties can help suppress volume expansion. Polyamide imide copolymer is a kind of polymer with the best comprehensive mechanical properties, for instance polyamide imide (PAI) [21] and polyimide (PI) [22]. The excellent mechanical properties mitigate the volume change of Si electrode, maintain the electric conduction network well, and eventually yield much improved cycle performance. Beyond that, the cross-linked polymers, PAA–CMC [23], PAA–polyvinyl alcohol (PVA) [24], and PAA–PAI [25], etc., exhibit further improvement. These mechanically robust binders which cooperatively work with the three-dimensional (3D) interconnected network can be expected to prevent the active material particles from sliding upon caused by continual volume change of silicon during cycling and effectively maintain the silicon-binder bond strength [23]. However, the cross-linked reaction between carboxyl and hydroxy for PAA–CMC and PAA–PVA, or between carboxyl and imides for PAA–PAI requires high activation energy and needs a heat treatment process over 100 °C in vacuum.

Here the development of an effective self-healing Alg–C-chitosan porous scaffold structure binder was reported. Alginate and chitosan are important bio-derived materials due to extensive sources and low price [26, 27]. Blending the two polymers at room temperature results in the spontaneous formation of a porous scaffold due to the occurrence of electrostatic interaction between carboxylate of Alg and protonated amines of C-chitosan [28]. The alginate–chitosan porous scaffold has been widely used in bioengineering, such as microcapsules [29], hydrocolloids for the intestinal delivery of protein drugs [30] and bone tissue engineering [31]. The alginate–C-chitosan composite polymer, with mechanical strength enhanced rigid porous scaffold structure and self-healing electrostatic interaction, may be beneficial to holding the Si-based electrode structure without fracture during charge–discharge cycling processes. For this purpose, the Alg–C-chitosan composite was applied as a polymer binder for silicon anodes in lithium-ion batteries in this study.

2 Experimental

2.1 Materials

Si nanopowders (SiNPs) with average particles size of 100 nm were purchased from Shanghai Shuitian Materials

Technology Co., China. Alg (mol mass of 8×10^5 – 12×10^5 g·mol⁻¹, medium viscosity) was purchased from Sigma-Aldrich, USA, dissolved in distilled water (2 wt%) standby. Alg is a linear polysaccharide copolymer that consists of two sterically different repeating units, (1,4)- β -D-mannuronic acid (M) and α -L-guluronic (G) in varying proportions. The ratio of M-to-G monoblocks in the Na alginate sample was 1.56. Carboxymethyl chitosan (carboxymethylation degree ≥ 60 %) was purchased from Nanjing Doulai Biological Technology Co., China, and dissolved in distilled water (5wt%) standby. PVDF (molar mass of $\sim 3 \times 10^6$ g·mol⁻¹) in N-methyl-2-pyrrolidone (NMP) and CMC/SBR (1:1 by weight) in distilled water was used as alternative binders for comparison.

For consistency, all electrodes contained SiNP, conducting additives (including 28 wt% super-P and 2 wt% carbon nanotubes (CNTs)), and polymeric binder with the weight ratio of 50:30:20. The electrode slurries were thoroughly mixed using a laboratory stirrer (FLUKO high shear dispersion emulsifying machine) for at least 1 h, coated on a piece of copper foil with ~ 8 μm in size, dried in air first at room temperature and then in vacuum at 105 °C for at least 8 h prior to use. The density of SiNP electrode was managed to be ~ 0.56 g·cm⁻³. The alginate–C-chitosan composite binder was formed in the process of slurry making. Active materials and conducting additives were firstly added to Alg aqueous solution and roughly mixed, and then C-chitosan was added with the same amount of Alg and fully mixed.

2.2 Measurements

Electrochemical tests were performed by using 2032 coin-type half cells assembled with lithium metal as the counter electrode in an Ar-filled glove box. The electrolyte consisted of 1 mol·L⁻¹ LiPF₆ in a mixture of ethylene carbonate, diethyl carbonate, and dimethyl carbonate (volume ratio of EC:DEC:DMC of 1:1:1). For long-term cycling tests, 10 vol% fluoroethylene carbonate (FEC) were added into the electrolyte solution. To clarify the effect of enhanced binder on the electrochemical performance, the cycling performance of Alg–C-chitosan binder was evaluated compared to the results for PVDF, CMC + SBR (1:1 by weight), Alg, and C-chitosan. Galvanostatic cycling tests of the SiNP electrodes were conducted at a constant current density of 100 mA·g⁻¹ in the voltage range of 0.02–1.00 V at room temperature (25 °C) on a CT2001A battery testing system. The specific capacity was calculated on the basis of the weight of the active materials.

Scanning electron microscopy (SEM) was performed on Hitachi S-4800, Japan. The sample was achieved by mixing Alg (2 wt%) and carboxymethyl chitosan (5 wt%) solution, and homogeneous blend solution of two polymers was formed under stirring at room temperature for 30 min and

then dried in air at room temperature till water was evaporated thoroughly. X-ray diffraction (XRD) patterns were performed on X-PerPRO MPO diffractometer (PANalytical) with Cu K α radiation source. The relative intensities were recorded within 2θ range of 5° – 80° at a scanning rate of $8^\circ\cdot\text{min}^{-1}$. Fourier transform infrared spectroscopy (FTIR) spectra were recorded on a Bruker Vector 22 FTIR spectrometer with 32 scans in the wavenumber range of 500 – 4000 cm^{-1} . The samples and KBr were fully dried prior to submission of samples by FTIR analyses to exclude the influence of water. The mechanical properties of the binders (Alg–C-chitosan, Alg, C-chitosan, and PVDF) were measured by a universal testing machine (CMT5000, MST). The specimens were cut to pieces with the same dimensions of $1\text{ cm} \times 10\text{ cm} \times 100\text{ }\mu\text{m}$, and the stretching velocity was fixed at $5\text{ mm}\cdot\text{min}^{-1}$.

3 Results and discussion

3.1 Alg–C-chitosan polymer binder

FTIR analysis was used to evaluate the interactions of Alg with C-chitosan. The FTIR spectra of C-chitosan, Alg, and

Alg–C-chitosan are shown in Fig. 1a. The characteristic peak of alginate is seen at 1620 cm^{-1} , corresponding to carbonyl (C=O) bond. The C-chitosan spectrum shows characteristic bands of amide-I (1640 cm^{-1}), amide-II (1560 cm^{-1}), and amino group (1173 cm^{-1}). Chitosan used in these experiments is deficiently deacetylated, and the double amide peaks correspond to the partial N-deacetylation of chitin [32, 33]. In the Alg–C-chitosan spectrum, the amide-I (1640 cm^{-1}) and amide-II (1560 cm^{-1}) bands are replaced by a new bond (1620 cm^{-1}), and the peak of the amino group (1173 cm^{-1}) is absent. The FRIT analysis shows that the amino groups on carboxymethyl chitosan interchain cross-linking carboxylic groups on alginate with the main electrostatic interaction, and forming a network matrix of Alg–C-chitosan copolymer complex [26]. Schematic illustration of cross-linking process of Alg and C-chitosan was shown in Fig. 1b. Moreover, the peaks at 1420 and 1070 cm^{-1} correspond to carboxyl –COOH and C–O stretching bands, respectively. The broad band around 3430 cm^{-1} was assigned to hydrogen bonded O–H stretching vibrations.

SEM image of the cross sections of Alg–C-chitosan film in Fig. 1c shows that this complex polymer has high condensed orientation and forms a porous scaffold structure.

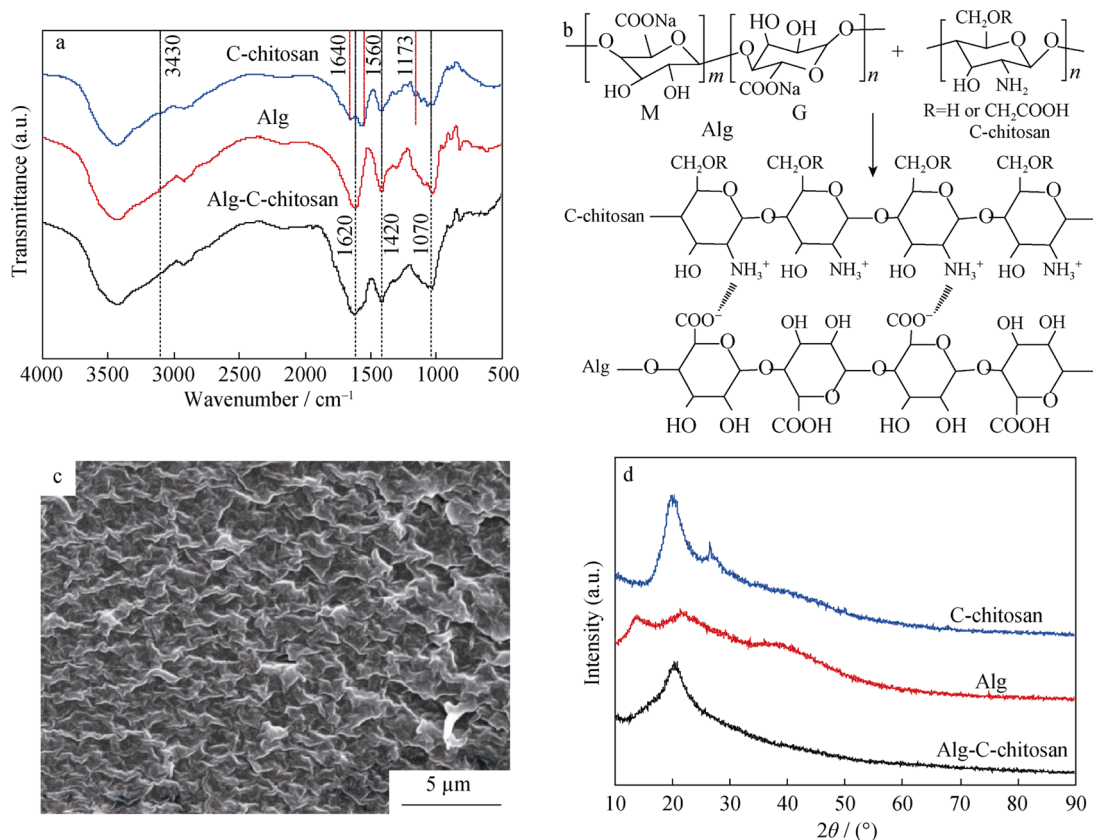


Fig. 1 FTIR spectra of C-chitosan, alginate, and alginate–C-chitosan complex **a**, schematic illustration showing cross-linking process between Alg and C-chitosan **b**, SEM image of cross section of Alg–C-chitosan film **c** and XRD patterns of Alg, C-chitosan, and Alg–C-chitosan complex **d**

Table 1 Tensile strength and elongation of polymer binders

Polymer binder	Tensile strength/MPa	Elongation at break/%
PVDF	32.43	50.6
Alg	42.28	6.8
C-chitosan	65.36	8.3
Alg–C-chitosan	89.68	6.2

Figure 1d presents the wide-angle XRD patterns of Alg, C-chitosan, and Alg–C-chitosan complex. The diffractogram of Alg consists of two crystalline peaks at $2\theta = 13.7^\circ$ and 23.0° [34]. Carboxymethyl chitosan exhibits a typical peak at $2\theta = 20.0^\circ$ [35], and the peak at $2\theta = 26.5^\circ$ may be caused by the intramolecular hydrogen bonding between amino groups and carboxylic groups. It is noticed that the crystalline peak at $2\theta = 26.5^\circ$ disappears for the diffractogram of Alg–C-chitosan complex, which is due to the interaction of the amino groups on C-chitosan and the carboxylic groups on Alg [36]. After cross-linking with Alg, the intensity peak at $2\theta = 20.0^\circ$ of C-chitosan is weakened drastically, and the two characteristic peaks of Alg disappear. It indicates that C-chitosan chains are realigned due to the cross-linking effect, resulting in a more amorphous structure.

It is well recognized that the mechanical property of polymeric binder is a major parameter that determines cycling performance of a Si anode [21, 22]. Better mechanical property is more beneficial to tolerating the internal mechanical stresses generated by the volume expansion of silicon nanoparticles and maintaining a consistent electrically conducting network during the electrochemical process. The tensile strength and elongation at break of the Alg–C-chitosan porous scaffold as well as pure carboxymethyl chitosan and sodium alginate in dry state are given in Table 1. From the results, it can be observed that the blend membrane exhibits higher tensile strength than the homopolymers. This enhancement may be attributed to the ionic-cross-linking between carboxymethyl chitosan and alginate to form an alginate–carboxymethyl chitosan complex. The polymer chains in the porous scaffold have electrostatic interactions with each other, restricting the mobility. This restriction results in an increase in the rigidity and the tensile strength.

3.2 Characterization of SiNP anode

As shown in Fig. 2a, the first cycle delithiation takes place around 0.4 V, which is consistent with previously reported values for other Si anodes; the first cycle lithiation potential shows a plateau profile at 0.02–0.10 V, consistent with the behavior of crystalline Si [9]. Importantly, the SiNP electrodes with different binders show remarkably different

specific capacities in the cycling. The Si–CMC/SBR, Si–Alg, and Si–C-chitosan electrodes show an excellent first charge/discharge capacities and initial coulombic efficiency (ICE) compared with Si–PVDF electrode: the first insertion of lithium capacities increases by 435, 547, and 412 $\text{mAh}\cdot\text{g}^{-1}$, and the ICE increases by 4.7 %, 5.4 %, and 6.0 %, respectively. The cycling performance of Si anode with different binders is shown in Fig. 2b. For non-functional PVDF binder, the electrode shows fast capacity fading ($160 \text{ mAh}\cdot\text{g}^{-1}$ after 100th cycling) with a very low ICE of 63.7 %. The relatively gradual decrease of capacity is observed for Si–CMC/SBR electrode, but the attenuation trend is similar to that of Si–PVDF electrode after 30th cycling. The Si anodes with functional Alg and C-chitosan binders show an excellent cycling stability compared to PVDF and CMC/SBR binders. Such consequence is coincident with former reports [16, 18].

It is clear that the electrochemical performance of Si–Alg–C-chitosan electrode is distinctly superior to the corresponding conventional electrodes (Fig. 2). Silicon composite anodes with the self-healing Alg–C-chitosan porous scaffold binder shows higher ICE of 74.5 % and superior capacities of 2565 and 1910 $\text{mAh}\cdot\text{g}^{-1}$ for the first insertion and extraction of lithium, respectively. Furthermore, this electrode also gives an excellent cycling stability, with a capacity of 750 $\text{mAh}\cdot\text{g}^{-1}$ remaining after 100th cycling, and the capacity retention compared with those of Si–Alg and Si–C-chitosan increases by 17.5 % and 15.5 %, respectively.

To confirm that the self-healing Alg–C-chitosan porous scaffold binder is robust enough for mechanical and electrical support, the thickness variation and surface topography change of the silicon electrodes during cycling were investigated by SEM. Figure 3 shows cross-sectional SEM images of Si–PVDF, Si–CMC + SBR, Si–Alg, and Si–Alg–C-chitosan electrodes before cycling and after 5th cycling. The thickness of Si–Alg–C-chitosan electrode increases to 16.9 μm (Fig. 3h) from its origin state of 15.4 μm (Fig. 3g) after 5th cycling, which is a $\sim 9.7\%$ volume change. In contrast, the Si–PVDF, Si–CMC + SBR, and Si–Alg electrodes undergo thickness increase of 66.5 %, 27.2 %, and 20.1 %, respectively. The smallest thickness change of the Si electrode with Alg–C-chitosan binder after 5th cycling is owing to the excellent mechanical properties of rigidly porous structure and self-healing electrostatic interaction of Alg–C-chitosan binder, which effectively alleviates the volume change of silicon and allows the reversible deformation of electrode during cycling. Moreover, the Si–PVDF electrode is delaminated from a Cu current collector and a large number of cracks could be observed from cross-sectional SEM images of Si–PVDF (Fig. 3b). It suggests that the poor mechanical property, weak binding force with active material, and Cu

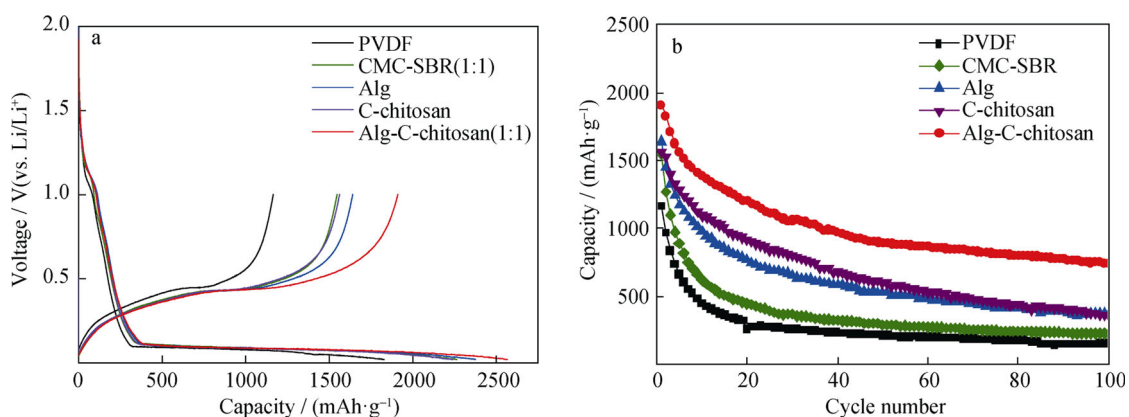


Fig. 2 Comparison of the first voltage profiles of Si anode with different binders **a** and cycling performance of Si anode with different binders **b**

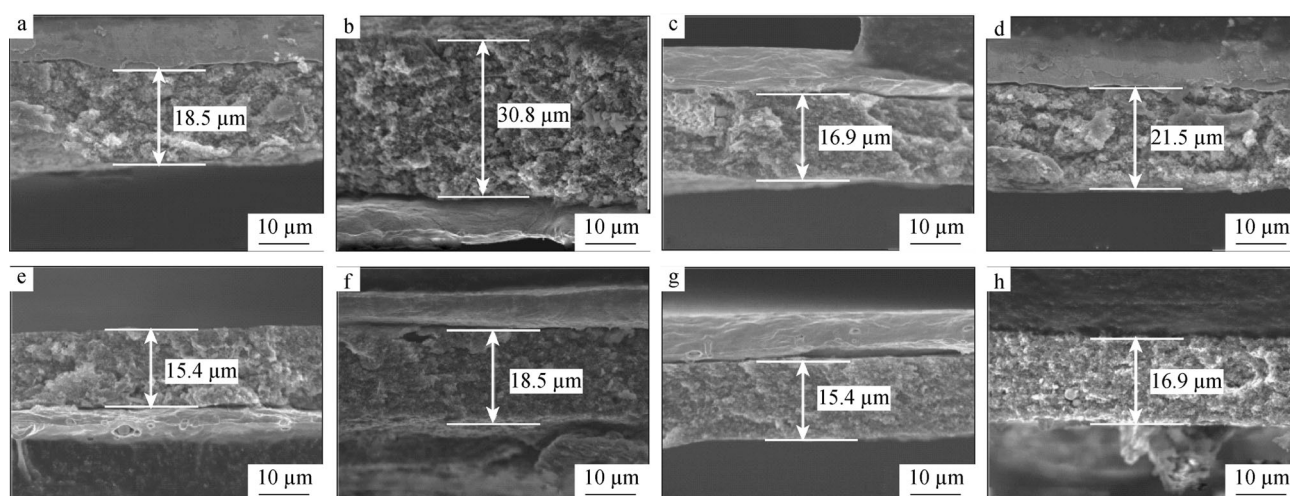


Fig. 3 SEM images of cross sections showing thickness change of **a** Si-PVDF, **c** Si-CMC + SBR, **e** Si-Alg and **g** Si-Alg-C-chitosan before cycling and **b** Si-PVDF, **d** Si-CMC + SBR, **f** Si-Alg and **h** Si-Alg-C-chitosan at end of 5th cycling

current collector of PVDF could be not enough to keep the Si-based electrode structure well, leading to the degradation of electrical conducting network, isolation of SiNP, and inferior electrochemical performance.

This can be further proved by the surface morphology change of the silicon electrodes. Figure 4 shows the surface microstructures of Si electrodes before cycling and after 30th cycling. It is found that all of the samples exhibit uniform particle distributions in their initial states before cycling. The clear changes are noted that (1) the electrodes lost the pores and change to the dense morphology and (2) some of the cracks are observed in the surface morphology of the Si-PVDF, Si-CMC + SBR, and Si-Alg electrodes after cycling. The dense morphology is considered to be due to pulverization of silicon particles from intrinsic volume change and constantly forming SEI on newly exposed surfaces subsequently [7]. The presence of the cracks may be caused by the poor mechanical strength of

the binders which cannot tolerate the structural stress produced by volume expansion of Si nanoparticles [22, 23]. In contrast, the intact pores structure and well-kept electrode micromorphology are found for the SiNP electrode with Alg-C-chitosan porous scaffold binder, even after 30th cycling. The intact pores structure enlarges the direct contact area with electrolyte and improves the efficiency of the lithium-ion transport. Meanwhile, the micromorphology of undamaged electrode is in favor of the formation of stabilized SEI, which plays an active role in the cycling life.

This excellent electrochemistry performance of the Si anode with self-healing Alg-C-chitosan porous scaffold binder can be explained by several reasons. First, carboxylic and amino function groups of the Alg-C-chitosan binder could interact with the hydroxyl groups on the silicon oxide surfaces by strong hydrogen bonding interactions. Second, synergistic effect on the enhanced mechanical properties of

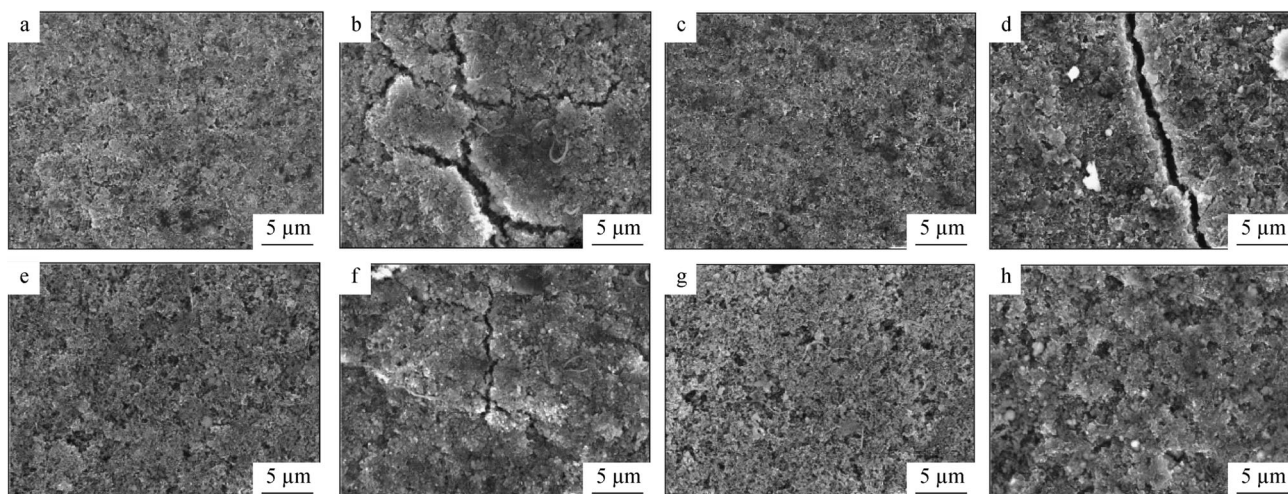


Fig. 4 SEM images of surface microstructures of **a** Si–PVDF, **c** Si–CMC + SBR, **e** Si–Alg and **g** Si–Alg–C–chitosan electrodes before cycling and **b** Si–PVDF, **d** Si–CMC + SBR, **f** Si–Alg and **h** Si–Alg–C–chitosan electrodes after 30th cycling

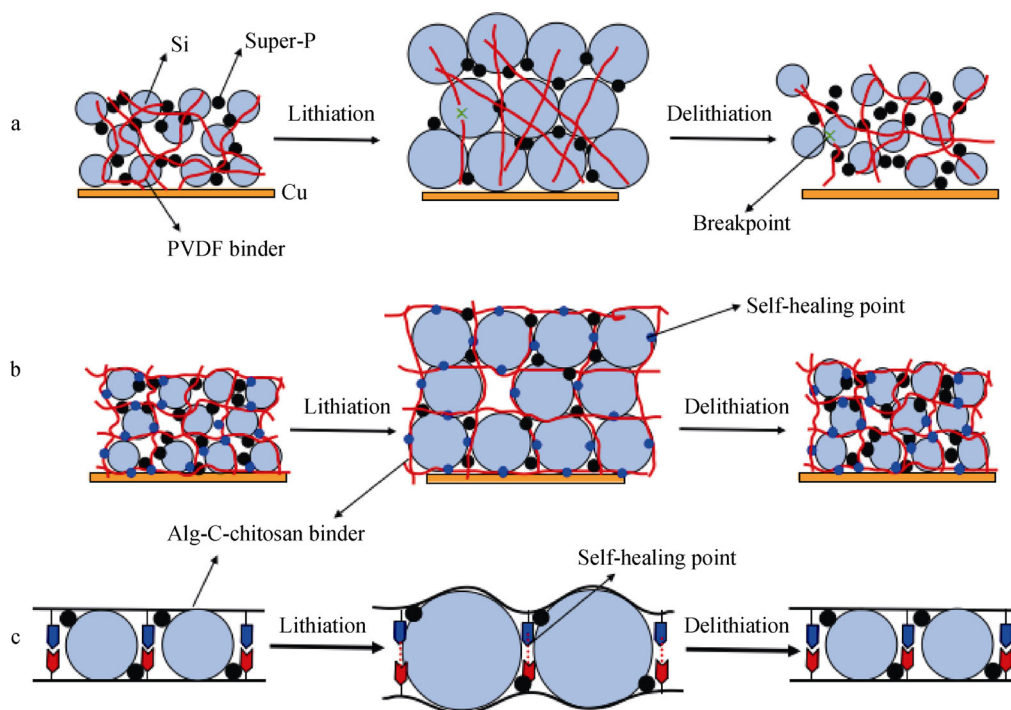


Fig. 5 Schematic illustrations of working mechanism of **a** PVDF and **b** Alg–C–chitosan porous scaffold binder on keeping mechanical integrity of Si electrode in cycling processes, and **c** details for self-healing working mechanism

the porous scaffold structure and self-healing electrostatic interaction of Alg–C–chitosan binder retard the breakdown of polymeric binder due to the structural stress produced by the volume expansion of silicon nanoparticles during the lithiation process (Fig. 5). Third, the cross-linking 3D network structure of the Alg–C–chitosan binder restricts active materials and conductive agent from sliding, which are

caused by continuous volume expansion/shrinkage of SiNP during cycling process. Fourth, the porous structure of the binder scaffold allows the Si particles to expand without the deformation of the electrode structure and increases ion transport in electrodes.

Furthermore, the self-healing Alg–C–chitosan porous scaffold binder was used to design a practical anode setting.

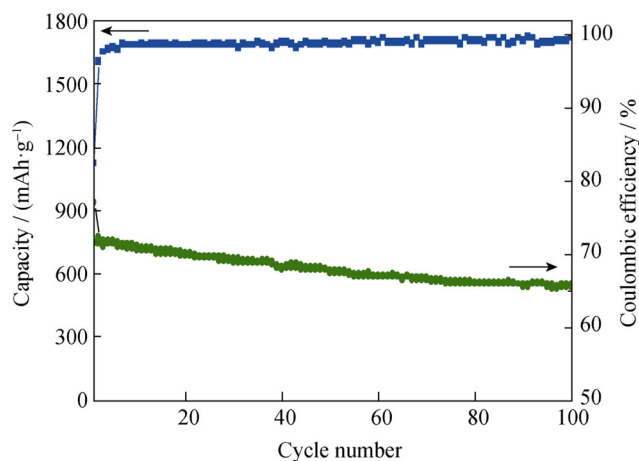


Fig. 6 Cycling performance of Si-Gr@C composite electrode

The working electrodes are made by a typical slurry method with Si/Gr@C composite, super-P, and Alg-C-chitosan binder with a mass ratio of 8:1:1, and the mass loading of active material (Si/Gr@C composite) is $>5 \text{ mg}\cdot\text{cm}^{-2}$. The cells were measured at current density of $40 \text{ mA}\cdot\text{g}^{-1}$ in the potential range of 0.005–2.000 V (vs. Li/Li⁺). As displayed in Fig. 6, the electrode exhibits charge/discharge capacities of 752/943 $\text{mAh}\cdot\text{g}^{-1}$ in the initial cycle with a relatively high ICE of 80.0 %. The ICE value increases to $\sim 98.0 \%$ at the third cycle and finally stabilizes at $\sim 99.5 \%$ in subsequent cycles. Moreover, after 160th cycling, the electrode preserves 60.6 % of the original capacity ($\sim 455 \text{ mAh}\cdot\text{g}^{-1}$). It is worth mentioning that the areal capacity of $\sim 3.76 \text{ mAh}\cdot\text{cm}^{-2}$ is superior compared with that in most reports [18, 37].

4 Conclusion

A self-healing alginate-carboxymethyl chitosan porous scaffold polymer based on the low-cost water-soluble alginate and carboxymethyl chitosan bio-derived precursors, as an excellent binder for silicon anodes in lithium batteries, was introduced. The electrostatic interaction between carboxylate ($-\text{COO}^-$) of Alg and protonated amines ($-\text{NH}_3^+$) of C-chitosan can be formed at room temperature during slurry, making process simple in use. The enhanced mechanical properties of the porous scaffold structure and self-healing electrostatic interaction of Alg-C-chitosan binder can tolerate the tremendous volume change of Si and maintain an integrated electrode structure during cycling process. Silicon composite anodes with the self-healing porous scaffold Alg-C-chitosan binder show an excellent cycling stability, with a capacity of $750 \text{ mAh}\cdot\text{g}^{-1}$ remaining after 100th cycling. It is noticeable that an extraordinary areal capacity of $3.76 \text{ mAh}\cdot\text{cm}^{-2}$

using the effective self-healing Alg-C-chitosan porous scaffold binder for Si/Gr@C composite anode was achieved. This novel developed water-soluble self-healing porous scaffold structure binder has a great potential to be used for high-capacity silicon anodes in next-generation lithium-ion batteries and also may be extended to other electrode materials that undergo large volume change.

Acknowledgments This study was financially supported by the National Natural Science Foundation of China (No. 51404032) and the National High Technology Research and Development Program of China (No. 2013AA050904).

References

- [1] Huggins RA. Lithium alloy negative electrodes. *J Power Sources*. 1999;81–82(1–2):13.
- [2] Wu H, Cui Y. Designing nanostructured Si anodes for high energy lithium ion batteries. *Nano Today*. 2012;7(5):414.
- [3] Key B, Morcrette M, Tarascon JM, Grey CP. Pair distribution function analysis and solid state NMR studies of silicon electrodes for lithium ion batteries: understanding the (de)lithiation mechanisms. *J Am Chem Soc*. 2010;133(3):503.
- [4] Boukamp BA, Lesh GC, Huggins RA. All-solid lithium electrodes with mixed-conductor matrix. *J Electrochem Soc*. 1981;128(4):725.
- [5] Chan CK, Peng H, Liu G, McIlwrath K, Zhang XF, Huggins RA, Cui Y. High-performance lithium battery anodes using silicon nanowires. *Nat Nanotechnol*. 2008;3(1):31.
- [6] Szczech JR, Jin S. Nanostructured silicon for high capacity lithium battery anodes. *Energy Environ Sci*. 2011;4(1):56.
- [7] Liu XH, Zhong L, Huang S, Mao SX, Zhu T, Huang JY. Size-dependent fracture of silicon nanoparticles during lithiation. *ACS Nano*. 2012;6(2):1522.
- [8] Jung DS, Hwang TH, Park SB, Choi JW. Spray drying method for large-scale and high-performance silicon negative electrodes in Li-ion batteries. *Nano Lett*. 2013;13(5):2092.
- [9] Wu H, Zheng G, Liu N, Carney TJ, Yang Y, Cui Y. Engineering empty space between Si nanoparticles for lithium-ion battery anodes. *Nano Lett*. 2012;12(2):904.
- [10] Li X, Cho JH, Li N, Zhang Y, Williams D, Dayeh SA, Picraux ST. Carbon nanotube-enhanced growth of silicon nanowires as an anode for high-performance lithium-ion batteries. *Adv Energy Mater*. 2012;2(1):87.
- [11] Fan Y, Zhang Q, Xiao Q, Wang X, Huang K. High performance lithium ion battery anodes based on carbon nanotube-silicon core-shell nanowires with controlled morphology. *Carbon*. 2013;59(7):264.
- [12] Liu N, Lu Z, Zhao J, Matthew MT, Lee HW, Zhao T, Cui Y. A pomegranate-inspired nanoscale design for large-volume-change lithium battery anodes. *Nat Nanotechnol*. 2014;9(3):187.
- [13] Komaba S, Shimomura K, Yabuuchi N, Ozeki T, Yui H, Konno K. Study on polymer binders for high-capacity SiO negative electrode of Li-ion batteries. *J Phys Chem C*. 2011;115(27):13487.
- [14] Munao D, Van Erven JWM, Valvo M, Garcia-Tamayo E, Kelder EM. Role of the binder on the failure mechanism of Si nano-composite electrodes for Li-ion batteries. *J Power Sources*. 2011;196(16):6695.
- [15] Li J, Lewis RB, Dahn JR. Sodium carboxymethyl cellulose a potential binder for Si negative electrodes for Li-ion batteries. *Electrochem Solid State Lett*. 2007;10(2):A17.

- [16] Yue L, Zhang L, Zhong H. Carboxymethyl chitosan: a new water soluble binder for Si anode of Li-ion batteries. *J Power Sources*. 2014;247(3):327.
- [17] Magasinski A, Zdyrko B, Kovalenko I, Hertzberg B, Burtovyy R, Huebner CF, Fuller TF, Luzinov I, Yushin G. Toward efficient binders for Li-ion battery Si-based anodes: polyacrylic acid. *ACS Appl Mater Interfaces*. 2010;2(11):3004.
- [18] Kovalenko I, Zdyrko B, Magasinski A, Hertzberg B, Milicev Z, Burtovyy R, Luzinov I, Yushin G. A major constituent of brown algae for use in high-capacity Li-ion batteries. *Science*. 2011;334(6052):75.
- [19] Bridel JS, Azais T, Morcrette M, Tarascon JM, Larcher D. Key parameters governing the reversibility of Si/carbon/CMC electrodes for li-ion batteries. *Chem Mater*. 2009;22(3):1229.
- [20] Hochgatterer NS, Schweiger MR, Koller S, Raimann PR, Wöhrle T, Wurm C, Winter M. Silicon/graphite composite electrodes for high-capacity anodes: influence of binder chemistry on cycling stability. *Electrochem Solid State Lett*. 2008;11(5):A76.
- [21] Choi NS, Yew KH, Choi WU, Kim SS. Enhanced electrochemical properties of a Si-based anode using an electrochemically active polyamide imide binder. *J Power Sources*. 2008;177(2):590.
- [22] Kim JS, Choi W, Cho KY, Byun D, Lim J, Lee JK. Effect of polyimide binder on electrochemical characteristics of surface-modified silicon anode for lithium ion batteries. *J Power Sources*. 2013;244(4):521.
- [23] Koo B, Kim H, Cho Y, Lee KT, Choi NS, Cho J. A highly cross-linked polymeric binder for high-performance silicon negative electrodes in lithium ion batteries. *Angew Chem Int Ed*. 2012;51(35):8762.
- [24] Song JX, Zhou MJ, Yi R, Xu T, Gordin ML, Tang DH, Yu ZX, Regula M, Wang DH. Interpenetrated gel polymer binder for high-performance silicon anodes in lithium-ion batteries. *Adv Funct Mater*. 2014;24(37):5904.
- [25] Yim T, Choi SJ, Jo YN, Kim TH, Kim KJ, Jeong G, Kim YJ. Effect of binder properties on electrochemical performance for silicon-graphite anode: method and application of binder screening. *Electrochem Acta*. 2014;136(8):112.
- [26] Lee KY, Mooney DJ. Alginate: properties and biomedical applications. *Prog Polym Sci*. 2012;37(1):106.
- [27] Rinaudo M. Chitin and chitosan: properties and applications. *Progr Polym Sci*. 2006;31(7):603.
- [28] Baruch L, Machluf M. Alginate-chitosan complex coacervation for cell encapsulation: effect on mechanical properties and on long-term viability. *Biopolymers*. 2006;82(6):570.
- [29] Li S, Wang XT, Zhang XB, Yang RJ, Zhang HZ, Zhu LZ, Hou XP. Studies on alginate–chitosan microcapsules and renal arterial embolization in rabbits. *J Control Release*. 2002;84(3):87.
- [30] George M, Abraham TE. Polyionic hydrocolloids for the intestinal delivery of protein drugs: alginate and chitosan—a review. *J Control Released*. 2006;114(1):1.
- [31] Li Z, Ramay HR, Hauch KD, Xiao D, Zhang M. Chitosan-alginate hybrid scaffolds for bone tissue engineering. *Biomaterials*. 2005;26(18):3919.
- [32] Mourya VK, Inamdar NN, Tiwari A. Carboxymethyl chitosan and its applications. *Adv Mater Lett*. 2010;1(1):11.
- [33] Sugimoto M, Morimoto M, Sashiwa H, Saimoto H, Shigemasa Y. Preparation and characterization of water-soluble chitin and chitosan derivatives. *Carbohydr Polym*. 1998;36(1):49.
- [34] Wang Q, Du Y, Hu X, Yang J, Fan L, Feng T. Preparation of alginate/soy protein isolate blend fibers through a novel coagulating bath. *J Appl Polym Sci*. 2006;101(1):425.
- [35] Salmon S, Hudson SM. Crystal morphology, biosynthesis, and physical assembly of cellulose, chitin, and chitosan. *Rev Macromol Chem Phys C*. 1997;37(2):199.
- [36] Kim JH, Lee YM. Synthesis and properties of diethylaminoethyl chitosan. *Polymer*. 1993;34(9):1952.
- [37] Zhao H, Wang ZH, Lu P, Jiang M, Shi FF, Song XY, Zheng ZY, Zhou X, Fu YB, Guerfi A, Xiao XC, Liu Z, Vincent SB, Karim Z, Liu G. Toward practical application of functional conductive polymer binder for a high-energy lithium-ion battery design. *Nano Lett*. 2015;14(11):6704.